RESEARCH ARTICLE | APRIL 13 2023

Study on the influence of processing variables under various tilting angles of laser nozzle and substrate on the deposition quality of the multi-axis laser metal deposition

Special Collection: Laser Additive Manufacturing Processes: From Cladding to Complex Parts

Dukyong Kim; Taehwan Ko; Seung Hwan Lee

Journal of Laser Applications 35, 022025 (2023)
https://doi.org/10.2351/7.0000979

Journal of Laser Applications ARTICLE scitation.org/journal/jla

Study on the influence of processing variables under various tilting angles of laser nozzle and substrate on the deposition quality of the multi-axis laser metal deposition

Cite as: J. Laser Appl. 35, 022025 (2023); doi: 10.2351/7.0000979
Submitted: 16 January 2023 · Accepted: 30 March 2023 ·
Published Online: 13 April 2023

Dukyong Kim,[a] Taehwan Ko,[b] and Seung Hwan Lee[c]

AFFILIATIONS

Department of Mechanical Engineering, Hanyang University, 222 Wangsimni-ro, Seongdong-gu, Seoul 04763, Republic of Korea

Note: This paper is part of the Special Collection: Laser Additive Manufacturing Processes: From Cladding to Complex Parts.
[a]**Electronic mail:** kdy0414@hanyang.ac.kr
[b]**Electronic mail:** taehwan007@hanyang.ac.kr
[c]**Electronic mail:** seunghlee@hanyang.ac.kr

ABSTRACT

This study developed a deposition guideline that considered the effect of processing variables, such as laser power, on the deposition quality at various tilting angles of laser nozzle and substrate when fabricating components of complex geometries like overhang and curved structures with the multi-axis laser metal deposition process. The guideline was based on analyzing the effect of processing variables, namely, laser power, beam diameter, and specific energy, on the deposition quality under six spatial variables. Spatial variables were defined by combining the angle of the substrate to the ground (0°, 45°, and 90°) with the angle of the laser nozzle to the substrate (90° and 45°). The bead contact angle and dilution were used as indexes of the deposition quality evaluation. If both the ideal ranges of the evaluation indexes are satisfied, the deposited material can exhibit high surface quality and geometrical accuracy. To prevent excessive dilution caused by the widened and flattened deposit under tilted laser nozzle conditions, a larger beam diameter, when compared to the state where the laser nozzle is perpendicular to the substrate, should be used. For a situation where the effect of the gravitational force is dominant, such as the substrate perpendicular to the ground, the laser power and the specific energy should be controlled simultaneously to maintain the ideal contact angle and dilution. In addition, the effect due to the change in the amount of melted powder on the cross-section geometry caused by beam diameter variation should be considered for every tilted motion.

Key words: multi-axis laser metal deposition, processing variable, spatial variable, bead contact angle, dilution

INTRODUCTION

Recently, with the advancement of additive manufacturing, laser metal deposition (LMD) has been widely applied in fabricating key components of the aerospace industry, such as propellers, turbine blades, and impellers.[1–4] A supporting structure is inevitable in constructing a propeller that overhangs from the central hub when using the conventional 3-axis of the x, y, and z LMD system. However, building a supporting structure that fits the product's shape precisely is challenging, and the additional removal process of the supporting structure leads to a prolonged process time.[5] When curved structures, such as the turbine blade and the impeller, are fabricated by using the 3-axis LMD system, the staircase effect, an effect in which the deposited layer notably appears under the inclined angle, occurs. This results in a rough surface and low geometrical accuracy of the deposit.[6] These drawbacks can be settled by tilting the laser nozzle or the substrate, thus eliminating the need for a supporting structure and minimizing the staircase effect. Therefore, to fabricate a component with no additional supporting structure and to minimize the staircase

TABLE I. Chemical composition of Inconel 625 powder (wt. %).

	Element (wt. %)							
Inconel 625	Ni	Cr	Fe	Mo	Nb + Ta	Co	Mn + Si	Al + Ti
Content	56.0	20.0–23.0	≤5.0	8.0–10.0	3.15–4.15	≤1.0	≤1.0	≤0.80

effect, a multi-axis LMD process in which the laser nozzle and the substrate can be tilted should be introduced.

The following matters should be considered when manufacturing structures of complex geometries, such as overhang and curved structures during the multi-axis LMD process.[7] Because of the tilted laser nozzle during the process, the change in the laser's power distribution onto the substrate can yield a deposit of an asymmetrical geometry. If the substrate is tilted, the geometrical accuracy can be deteriorated due to the gravitational force applied to the melted liquid-state powder. For these reasons, to enhance the geometrical accuracy and deposition quality of the components when using the multi-axis LMD system, several researchers studied the effect of laser nozzle and substrate tilting on the shape of the deposited material based on the flow behavior of the melted powder. Zhu *et al.*[8] proposed a cross-section analysis of the single-layer structure in conditions where the laser nozzle and substrate were tilted while fixing the laser nozzle's posture perpendicular to the substrate. They showed that the bead width remained constant until the laser nozzle and the substrate were both tilted up to 150° from the ground and that the bead height was maintained up to a 90° tilt but then decreased afterward. In addition, Pedro *et al.*[9] tilted the laser nozzle and substrate both separately and together up to 30° and analyzed the resulting deposition characteristics. Based on their experiments, as the relative angle between the laser nozzle and substrate decreased, the bead width increased while its height decreased. The preceding researchers have studied the influences of laser nozzle and substrate tilting on the shape of the deposited material using only the optimal processing variables they have insisted on. However, for components used not only in the aerospace fields but also in other industrial fields, within the same part, depending on their specific usage, the size, thickness, and length at each location differs. Therefore, during the multi-axis LMD process of each separate layer, processing variables, such as laser power, beam diameter, and scanning speed, must be simultaneously controlled under various tilting angles of the laser nozzle and the substrate. Up to this point, for fabricating components of different shapes, not much research has analyzed the effect of processing variables on the cross-section geometry and the quality of the deposited material for tilted laser nozzle and substrate conditions.

Therefore, this study established a deposition guideline that considered the effect of the change in the processing variables on the deposition quality under tilted laser nozzle and substrate conditions. Following the guideline ensures an excellent deposition quality of components with complex geometries, such as the overhang or curved structures, made using the multi-axis LMD process. In establishing the guideline, spatial variables, which are related to the posture of the substrate and the laser nozzle, and the processing variables were defined. The spatial variables were determined by combining the angle between the substrate and the ground 0°, 45°, and 90° with the angle between the laser nozzle and the substrate 90° and 45°. The processing variables were laser power, beam diameter, and specific energy. After the deposition process, the effects of the change in the variables on the cross-section geometry and the deposition quality have been investigated. Bead contact angle and dilution were chosen as the evaluation indexes in judging the deposition quality. They were used to assess whether a deposited material with superior surface quality and no internal defects, such as inter-run porosity between layers and good metallurgical bonding with the substrate, could be fabricated. Then, the correlation between the evaluation indexes and the spatial and processing variable were analyzed using the two evaluation indexes. Based on these analyses altogether, the deposition guideline was established.

EXPERIMENTAL SETUP AND METHODS

Multi-axis LMD system

The multi-axis LMD system was mainly configured with a laser, a powder feeder, a 6-axis robot, and a 1-axis zig. For the laser, TruDisk 4000 (TRUMPF, Germany) with a maximum power output of 4 kW at a wavelength of 1030 nm was used. The powder feeder (Medicoat, Switzerland) supplied the metal powder at a feed rate of 17.5 g/min on top of the substrate surface where the laser was irradiated. The powder's focal spot diameter was 2.5 mm. The 6-axis robot (KUKA, Germany) was used to tilt and move the laser nozzle. The 1-axis zig was used to rotate the substrate, with a maximum of 90° tilt angle from the ground.

Materials

The metal powder used for the LMD process was a nickel-based superalloy Inconel 625 (Sandvik Osprey, England) with a

TABLE II. Chemical composition of stainless steel 316L substrate (wt. %).

	Element (wt. %)							
Stainless steel 316L	Ni	Cr	Fe	Mo	P + S	C	Mn + Si	Cu
Content	10.09	16.63	Bal.	2.05	≤0.03	0.016	1.75	0.26

particle diameter of 53–150 μm. For the substrate, stainless steel 316L with a dimension of $100 \times 20 \times 10\ mm^3$ was used.[10,11] Because of Inconel 625's outstanding mechanical properties at high temperatures and stainless steel 316L's superior corrosion-resistant properties, the two materials are used together in building jet engines and exhaust pipes.[12–15] The chemical composition of the Inconel 625 powder and stainless steel 316L substrate is shown in Tables I and II each.

Spatial and processing variables

In this study, six spatial variables were introduced by combining the substrate's three postures, A, B, and C, in which each posture referred to the angle between the substrate and the ground (0°, 45°, and 90°) with the angle θ between the laser nozzle and the substrate (90° and 45°). Each spatial variable's name was given by combining the substrate's posture with the angle θ between the laser nozzle and the substrate.

1. A—90°, A—45° [Figs. 1(a) and 1(b)]: For A posture in which the substrate lay parallel to the ground, θ between the laser nozzle and the substrate was 90° and 45° each.
2. B—90°, B—45° [Figs. 1(c) and 1(d)]: For B posture in which the substrate was tilted 45° from the ground, θ between the laser nozzle and the substrate was 90° and 45° each.
3. C—90°, C—45° [Figs. 1(e) and 1(f)]: For C posture in which the substrate was perpendicular to the ground, θ between the laser nozzle and the substrate was 90° and 45° each.

Based on initial experiments, the processing variables' values were determined for analyzing the effects of the processing variables on the deposition quality. The values for each laser power and beam diameter were set to 600, 900, or 1200 W and 1, 2, or 3 mm, respectively. The values of the specific energy were fixed to 45, 60, and 75 J/mm^2. Specific energy was defined by the equation shown below:[16]

$$\text{Specific energy (J/mm}^2) = \frac{\text{Laser power (W)}}{\text{Beam diameter (mm)} \times \text{Scanning speed (mm/s)}}.$$

Table III shows the values of the processing variables used for this experiment. For example, at A—90°, the combination of laser power 600 W, beam diameter 1 mm, specific energy of 45 J/mm^2 was used to perform the LMD process. Therefore, 27 sets of processing variables were used under six spatial variables.

Deposition method and cross-section characteristics

In this study, single-layer structures were deposited on top of the substrate to evaluate the deposited material's quality under various spatial and processing variables. Then, the bead characteristics for bead cross-section geometry analysis and deposition quality evaluation were measured. Figure 2(a) shows a three-dimensional schematic of a single-layer process performed specimen. The metal powder delivered through the laser nozzle was deposited at a length of 60 mm in the laser scanning direction. The cross-section analysis of the deposited single-layer was performed at three locations; the center point and two points that are 8 mm apart from the center point, as depicted in Fig. 2(a). An optical microscope (OM) (Olympus, Japan) was used to capture the cross-section images at each location. The two-dimensional bead cross-section schematic depicted in Fig. 2(b) indicates the bead characteristics for cross-section geometry analysis and deposition quality evaluation. The bead characteristics for cross-section geometry analysis were the average values of bead width, bead height, and penetration depth measured at three cross-section analysis locations. The evaluation indexes used for deposition quality evaluation were left and right bead contact angle (β_l, β_r) and dilution (D). The bead contact angle (β) is the dihedral angle between the substrate's surface and the plane tangential to the deposited material. It can be obtained at both ends of the bead. Dilution, as shown in Fig. 2(b), indicates the percentage of the melted powder's area inside the substrate as indicated by the dark color among the whole bead area. Dilution can be expressed as the equation shown below (A_m is the melted powder inside the substrate and A_b is the area of the whole bead area subtracted by A_m),

$$\text{Dilution } (D) = \frac{A_m}{A_m + A_b} \times 100\ (\%).$$

For the two indexes used for deposition quality evaluation, if the contact angle is larger than 80°, the deposit's surface quality may deteriorate, and during the deposition process with overlapping layers, inter-run porosity can be formed inside the final product.[17] When dilution is lower than 10%, the deposit can be readily torn off from the substrate because of weak metallurgical bonding between the substrate and the deposited material.[18] Dilution exceeding 30% may be problematic because it may lead to an unstable LMD process that yields deposits with poor geometrical accuracy.[19] Therefore, this study defined and applied the ideal ranges for contact angle ($\beta < 80°$) and dilution ($10\% < D < 30\%$) for establishing a guideline needed when fabricating a component with a superior deposition quality.

TABLE III. Processing variables used for this experiment.

Processing variable (unit)	Value
Laser power (W)	600, 900, 1200
Beam diameter (mm)	1, 2, 3
Specific energy (J/mm^2)	45, 60, 75

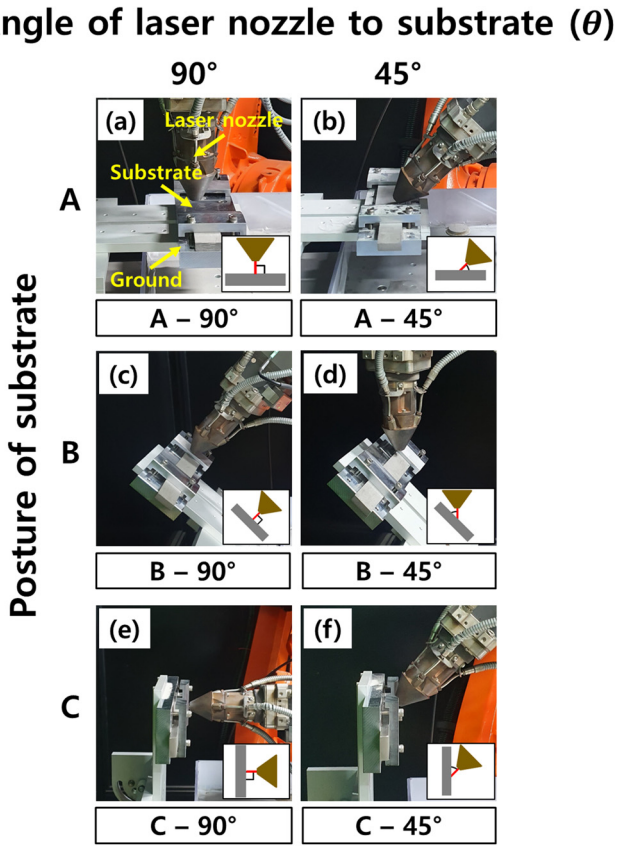

FIG. 1. Spatial variables defined by combining the substrate's posture (A, B, C posture) with the angle (θ) between the laser nozzle and the substrate. (a) A posture (the angle between the substrate and the ground: 0°) when θ is 90° (A—90°), (b) A posture (the angle between the substrate and the ground: 0°) when θ is 45° (A—45°), (c) B posture (the angle between the substrate and the ground: 45°) when θ is 90° (B—90°), (d) B posture (the angle between the substrate and the ground: 45°) when θ is 45° (B—45°), (e) C posture (the angle between the substrate and the ground: 90°) when θ is 90° (C—90°), (f) C posture (the angle between the substrate and the ground: 90°) when θ is 45° (C—45°).

RESULTS AND DISCUSSION

Cross-section analysis

Effect of laser nozzle tilting under A posture

In this section, for a substrate in A posture in which the angle between the substrate and the ground was 0°, for θ set as 90° and 45°, two spatial variables A—90° and A—45° were compared to analyze the effect of laser nozzle tilting on the bead cross-section geometry.

Figure 3(a) shows the bead width, bead height, and penetration depth for spatial variables at A—90° and A—45°. The bead width at A—90° and A—45° during beam diameter of 1 mm was not greatly affected by the change in the laser power and specific energy. When a beam diameter of 1 mm was used, the amount of powder fed inside the laser beam diameter was low. Therefore, because of the low amount of powder melted, the processing variable did not affect the cross-section geometry significantly. At a beam diameter of 1 mm, the bead width of A—45° was wider than A—90°, and the bead width difference between the two spatial variables was almost maintained the same even when the laser power was increased. For a beam diameter of 2 mm, the bead width at A—90° and A—45° widened as the laser power increased. When the specific energy increased at a fixed laser power and beam diameter condition, the bead width at A—45° widened, while the bead width at A—90° did not change much. The specific energy increase under fixed laser power and beam diameter condition referred to the decrease in the scanning speed. Therefore, the effect of scanning speed on the bead width was low when θ was 90° and high when θ was 45° in which its effect increased with lower scanning speed. For every laser power, a beam diameter of 2 mm, and specific energy 60, 75 J/mm^2, the bead width was wider for A—45° than A—90° as depicted in the OM image of Fig. 3(b). In addition, the bead width difference between A—90° and A—45° did not greatly change even when the laser power was increased. However, when the specific energy was 45 J/mm^2 at a beam diameter of 1 mm, the bead width for the two spatial variables was similar. The bead width variation due to laser nozzle tilting did not occur at this condition because when the laser power and beam diameter were fixed, the scanning speed at specific energy of 45 J/mm^2 was higher than specific energy of 60, 75 J/mm^2 condition. The phenomenon in which the bead width of A—90° and A—45° was similar at a beam diameter of 2 mm, specific energy of 45 J/mm^2 did not occur at the beam diameter 1 mm condition. This was because the laser power density decreased as the beam diameter increased, which led to a decrease in the effect of the laser nozzle tilting on the beam cross-section geometry. For a beam diameter of 3 mm, the bead width of A—90° and A—45° widened as laser power increased, just like the beam diameter 2 mm condition. Also, the effect of specific energy under fixed laser power and beam diameter on the bead width appeared at A—45° while insignificant at A—90°. At a beam diameter of 3 mm, except for laser power 600 W, and specific energy 45, 60 J/mm^2, the bead width of A—45° was sufficiently greater than A—90°. Especially, unlike beam diameter 1 and 2 mm conditions, when a beam diameter of 3 mm was used, the bead width difference between A—90° and A—45° was small at laser power 600 W and specific energy 60 J/mm^2. This was because of the decrease in laser power density when the beam diameter was increased.

For bead height under a beam diameter of 1 mm, as the laser power increased, the bead height of A—90° decreased. For the bead height of A—45°, the height decreased when the laser power increased from 600 to 900 W, which is comparable to A—90°. However, the bead height of A—45° increased when the laser power was increased from 900 to 1200 W. The reason for the bead height's increase at A—45° (900–1200 W) was because when a bem diameter of 1 mm was used, the bead width's variation with respect to the laser power was minimal, and the melted powder tended to accumulate in the direction of the laser nozzle rather than being diluted in the direction perpendicularly inward to the substrate. When a beam diameter of 2 mm was used, all the bead heights for A—90° and A—45° decreased as the laser power increased. As the specific energy increased under fixed laser power and beam diameter

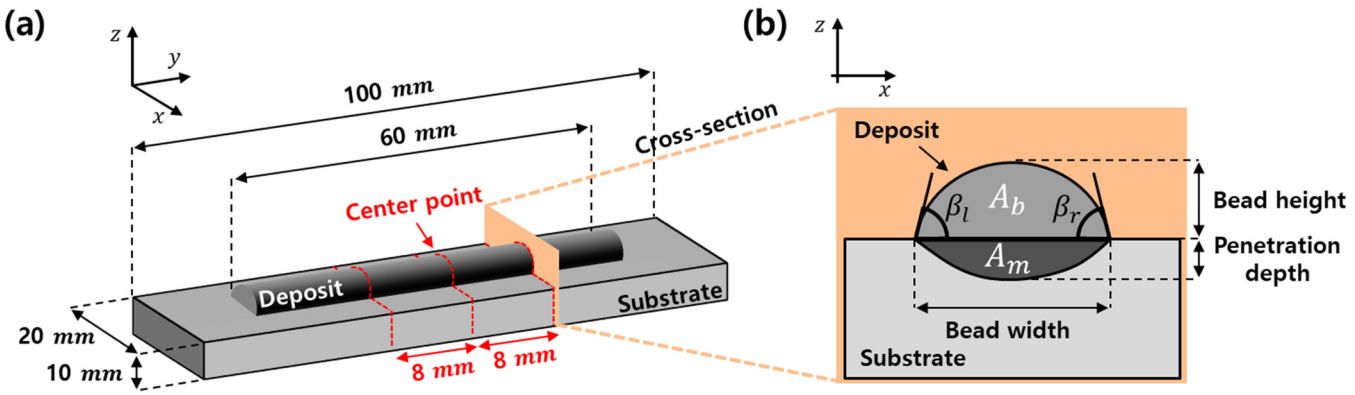

FIG. 2. Deposited single-layer; (a) three-dimensional schematic of the single-layer and the location for cross-section analysis and (b) two-dimensional schematic of the bead cross-section and the bead characteristics for cross-section geometry analysis and deposition quality evaluation.

conditions, the bead height of A—90° increased while the bead height for A—45° was not significantly affected. Therefore, under a beam diameter of 2 mm, the effect of scanning speed on the bead height was low when θ was 45° and high when θ was 90°, while its effect increased as the scanning speed decreased. The bead height of A—90° was higher than A—45° at laser powers 600, 900, 1200 W, a beam diameter of 2 mm, and specific energy 60, 75 J/mm^2. However, at specific energy 45 J/mm^2, the bead height difference between the two spatial variables was marginal. The reason for this was equivalent to the reason why the bead width between A—90° and A—45° was similar under the same processing variable set. For a beam diameter of 3 mm, like 2 mm, the bead height of A—90° and A—45° decreased as the laser power increased. Under fixed laser power and beam diameter condition, as the specific energy increased, the bead height for both θ at 90° and 45° increased. When θ was 45°, unlike beam diameter 1 and 2 mm conditions, at a beam diameter of 3 mm, there existed a difference in bead height when the specific energy changed. This phenomenon was because, under fixed laser power and specific energy, the scanning speed at a beam diameter of 3 mm was lower than at 2 mm. Therefore, because of the low scanning speed at a beam diameter of 3 mm, the effect of scanning speed on the bead height intensified at A—90°. Overall, for every spatial variable, the bead height increased as the beam diameter increased from 1 to 3 mm because the increase in the beam diameter yielded an increase in the amount of melted powder as well as the decrease in the scanning speed.

Regardless of laser nozzle tilting, penetration depth at A posture did not significantly change under the variation of laser power and specific energy. However, as the beam diameter increased from 1 to 3 mm, the laser power density decreased, and the amount of melted powder increased, thereby a shorter penetration depth was developed.

Effect of laser nozzle tilting under B posture

For a substrate in B posture in which the substrate was tilted 45° from the ground, B—90° and B—45° were compared to investigate the effect of laser nozzle tilting on the bead cross-section geometry.

In Fig. 4(a), the effect of the laser nozzle tilting at B posture on the cross-section geometry was analyzed. Under beam diameters 1, 2, and 3 mm, the bead width of B—90° and B—45° widened as the laser power and beam diameter increased. Under fixed laser power and beam diameter conditions, the bead width was not significantly affected by the change in specific energy for both θ (90° and 45°) conditions. Therefore, when θ was 45°, for B posture, the effect of scanning speed on the bead width was insignificant when compared to A posture.

The bead height of B—90° and B—45° under beam diameters of 1, 2, and 3 mm decreased as the laser power increased. When a larger beam diameter was used, the height increased. In addition, as the specific energy increased at a fixed laser power and diameter condition, the bead height for both spatial variables increased. Therefore, regardless of laser nozzle tilting, for substrate in B posture, the scanning speed had an influence on the bead height for every beam diameter condition.

Penetration depth at B posture did not significantly change under different laser power and specific energy. In this case, like the A posture, the penetration depth decreased when a larger beam diameter was used.

Moreover, in this study, the effect of laser nozzle tilting under B posture and A posture was compared to investigate the effect of substrate tilting on the cross-section geometry. As shown in the OM image of Fig. 4(b), the bead width and height between B—90° and B—45° was comparable. At B—90° and B—45°, the maximum bead width and height difference with or without laser nozzle tilting was 0.6 and 0.3 mm, respectively. On the other hand, at A posture [Fig. 3(a)], the maximum bead width and height difference with or without laser nozzle tilting was 1.1 and 1.2 mm each. The maximum bead width and height difference was smaller at the B posture when compared to the A posture because the influence of laser nozzle tilting on deposit geometry was larger than substrate tilting. At B—45°, the melted powder flowed along the inclined substrate, but solidified rapidly, yielding bead geometry comparable

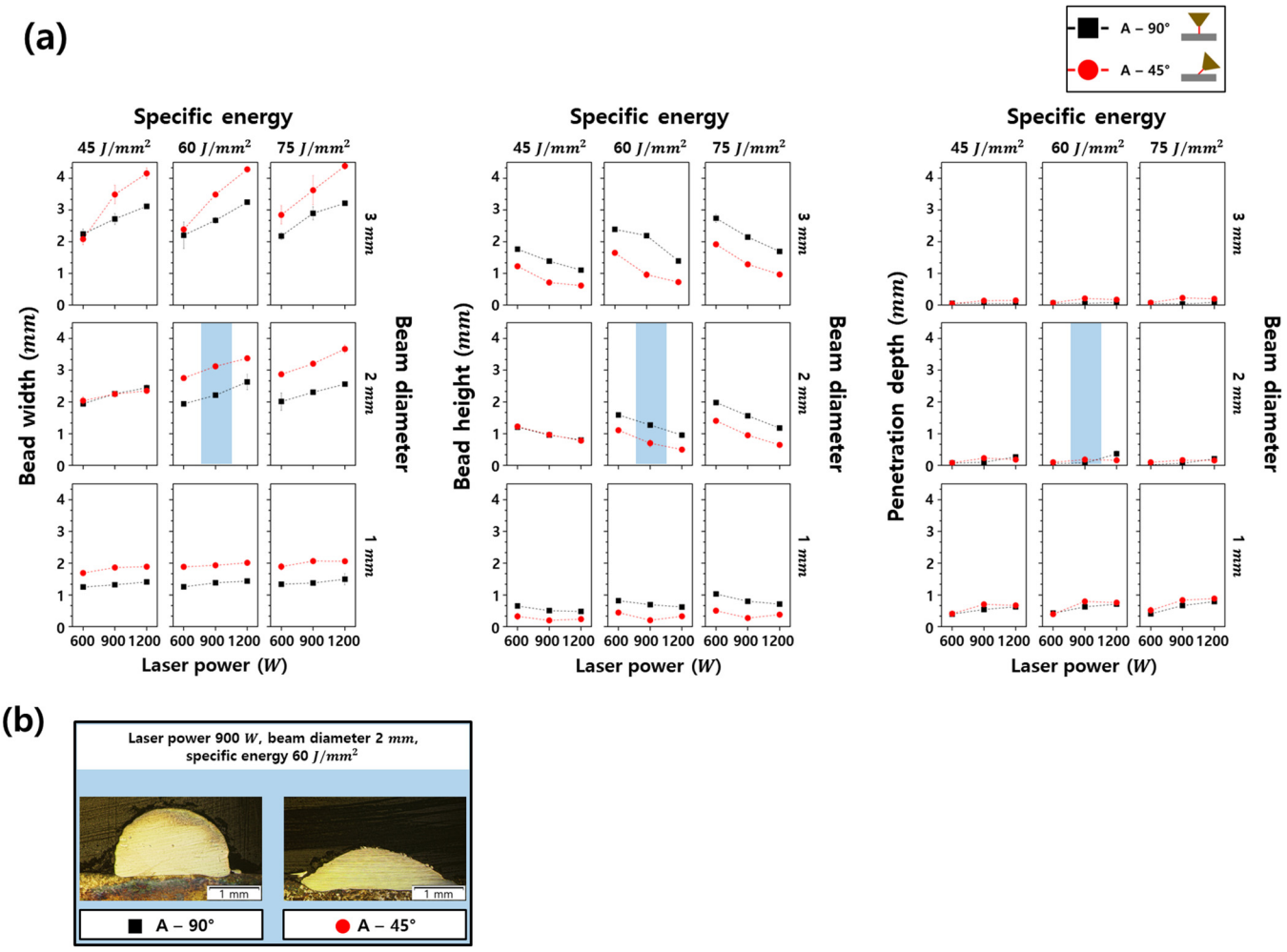

FIG. 3. Analysis and comparison of the laser nozzle tilting effect on bead cross-section geometry at A posture; (a) bead width, bead height, and penetration depth for A—90° and A—45° under every processing variable and (b) OM image of A—90° and A—45° at laser power 900 W, beam diameter 2 mm, and specific energy of 60 J/mm^2.

to B—90°. However, at A—45°, the overall bead geometry widened and flattened than at A—90° by laser nozzle tilting, which implied that laser nozzle tilting was a more dominant factor in changing the geometry of the deposit than substrate tilting.

Effect of laser nozzle tilting under C posture

For a substrate in C posture in which the substrate was perpendicular to the ground, C—90° and C—45° were compared to investigate the effect of laser nozzle tilting on the bead cross-section geometry.

In Fig. 5(a) by comparing two spatial variables at C posture with θ fixed at 90° and 45°, the spatial and processing variable's influence on the cross-section geometry was investigated. When a beam diameter of 1 mm was used for C—90° and C—45°, because the amount of melted powder was low, the effect of laser power and specific energy under fixed laser power and beam diameter on the bead width was insignificant. At a beam diameter of 1 mm, the bead width of C—45° was wider than C—90° regardless of any laser power used. For a beam diameter of 2 mm, whether the laser nozzle was tilted or not, except for laser power 600 W and specific energy of 60 and 75 J/mm^2, the bead width widened as the laser power increased. In addition, the bead width of C—45° was well wide enough than C—90°. Unlike a beam diameter 1 mm, when 2 mm was used at laser power 600 W, the bead width for the two spatial variables were similar at specific energy of 60 J/mm^2, and C—45° was slightly shorter than C—90° at specific energy of 75 J/mm^2. These specific processing variable sets at beam diameter 2 mm had lower laser power density compared to beam diameter 1 mm and had the most insufficient laser power, while the amount

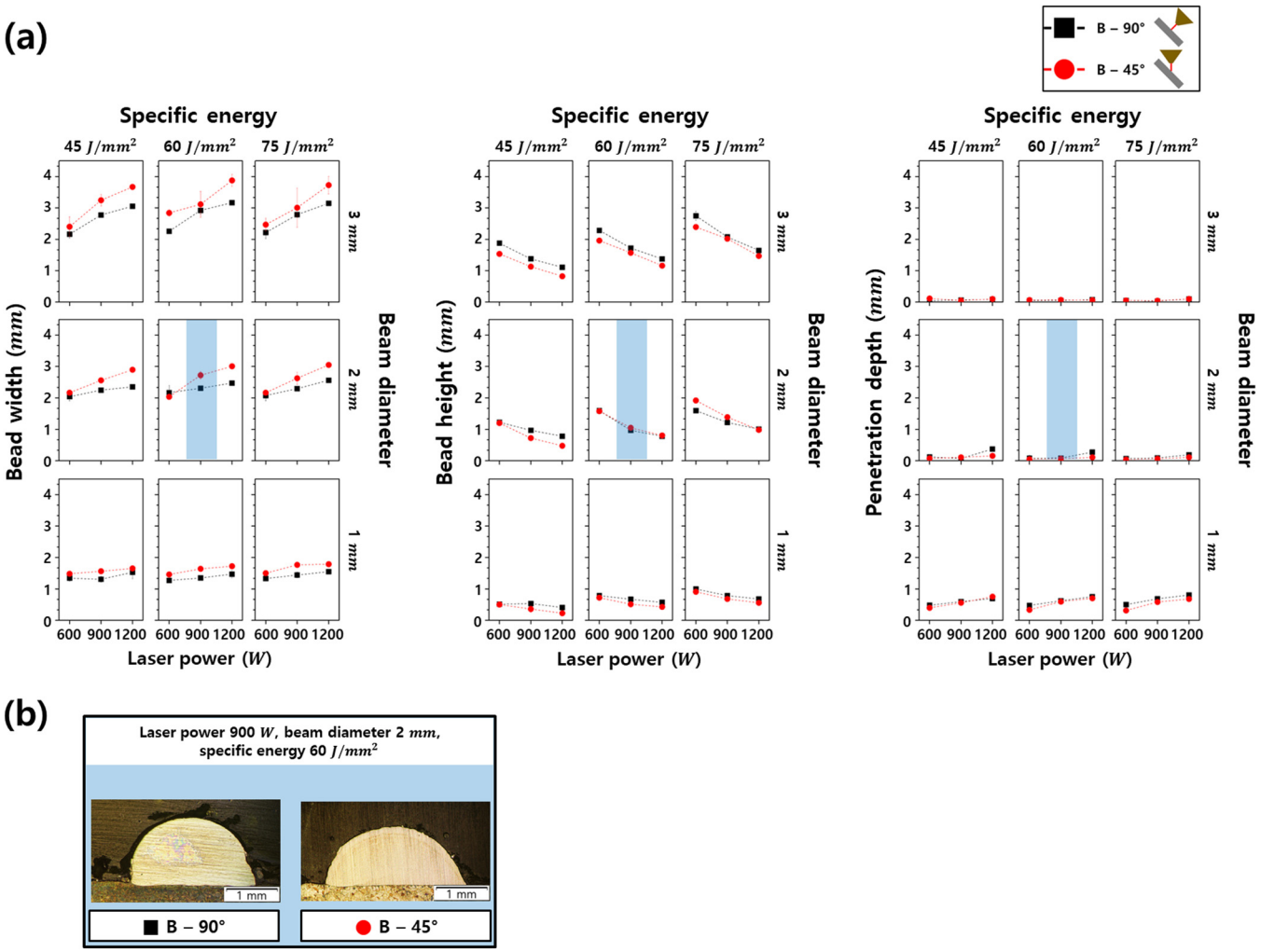

FIG. 4. Analysis and comparison of the laser nozzle tilting effect on bead cross-section geometry at B posture; (a) bead width, bead height, and penetration depth for B—90° and B—45° under every processing variable and (b) OM image of B—90° and B—45° at laser power 900 W, beam diameter 2 mm, and specific energy of 60 J/mm^2.

of powder fed over unit scanning length was large because of the low scanning speed than specific energy of 45 J/mm^2. Therefore, a large amount of melted power was not diluted enough, which led to a spherical shape formed on top of the substrate. This shape led to a short bead width for this processing variable set. For the same following reasons, at a beam diameter of 3 mm, the bead width of C—45° appeared shorter than C—90° at laser power 600 W, specific energy of 60 and 75 J/mm^2. Especially at laser power 600 W and specific energy of 75 J/mm^2, the bead width difference between C—90° and C—45° was the largest by 1.8 mm.

When a beam diameter of 1 mm was used, the bead height at C—90° and C—45° decreased when the laser power increased. However, at beam diameters 2 and 3 mm, the bead height instead increased when the laser power was increased from 900 to 1200 W. Notably, at a beam diameter of 3 mm and specific energy of 75 J/mm^2, the bead height increased the most by 1.3 mm at beam diameters 2 and 3 mm. The reason for the increase in the bead height under laser power increment from 900 to 1200 W was because, as shown in the OM image of Figs. 5(b-1) and 5(b-2), the increase in beam diameter caused a decrease in heat energy transferred to the substrate, which led to a decline in the amount of powder diluted in the substrate. Then, the melted powder rapidly solidified in the laser nozzle's direction, which led to a bead height increase.

For the penetration depth, like the A and B postures, at C posture, the penetration depth was not significantly affected by processing variables regardless of laser nozzle tilting. For the same previous reason for A and B posture, the penetration depth decreased when the beam diameter was increased.

Among the six spatial variables, the spatial variable affected the most by the laser nozzle tilting and gravitational force was

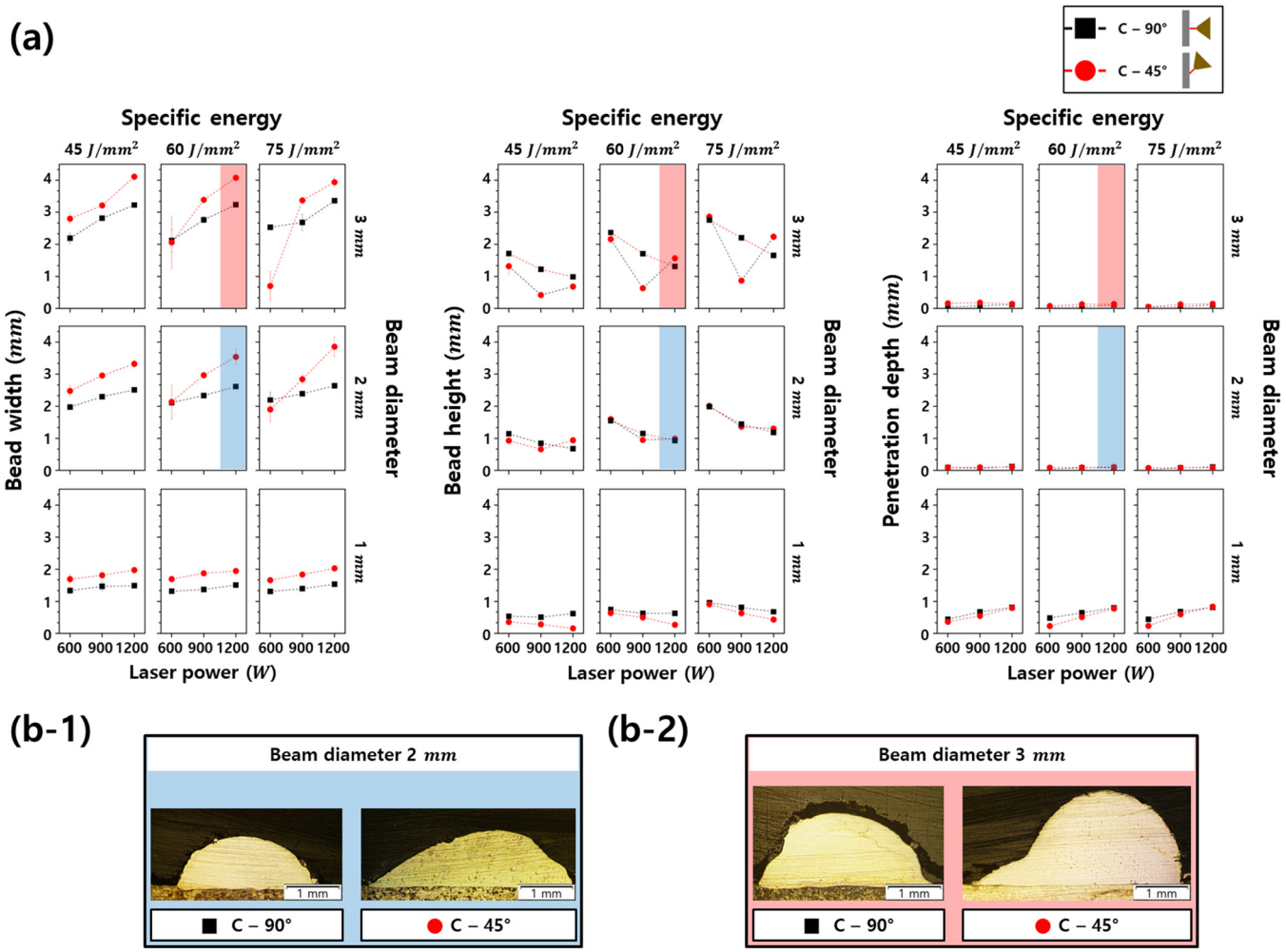

FIG. 5. Analysis and comparison of the laser nozzle tilting effect on bead cross-section geometry at C posture; (a) bead width, bead height, and penetration depth for C—90° and C—45° under every processing variable, (b-1) OM image at laser power 1200 W, beam diameter 2 mm, and specific energy of 60 J/mm^2 (blue colored), (b-2) OM image at laser power 1200 W, beam diameter 3 mm, and specific energy of 60 J/mm^2 (red colored).

investigated. At C—45° when compared with C—90°, for laser power 600 W, beam diameter 3 mm, and specific energy of 75 J/mm^2, the bead width was very small while the bead width and penetration depth were similar to each other. This type of cross-section geometry provided the most vulnerable condition where the deposit may fall apart from the substrate. Notably, during the cutting process for cross-section analysis for this variable set, the deposit fell apart from the substrate at one of the specimens. On top of that, except for C—45° at laser power 600 W, beam diameter 3 mm, and specific energy of 75 J/mm^2, for the remaining five spatial variables, the deposit remained attached to the substrate well. Therefore, C—45° was the spatial variable affected the most by laser nozzle tilting and gravitational force among the six spatial variables.

Effect of gravitational force under A, B, and C posture

For spatial variables, with θ fixed at 90°, A, B, and C postures were compared to analyze the effect of gravitational force on the deposit's cross-section geometry.

Figure 6(a) shows the cross-section geometry characteristics at A—90°, B—90°, and C—90°. The bead width for A—90°, B—90°, and C—90° widened as the laser power and beam diameter increased, while the bead height decreased as laser power increased and the bead height increased as the beam diameter was enlarged. The maximum bead width, bead height, and penetration depth difference between the three spatial variables were 0.2 0.3, and less than 0.1 mm, respectively. Therefore, the bead cross-section geometry was similar under various processing variables at A—90°, B—90°, and C—90°. The reason for this similarity can be confirmed

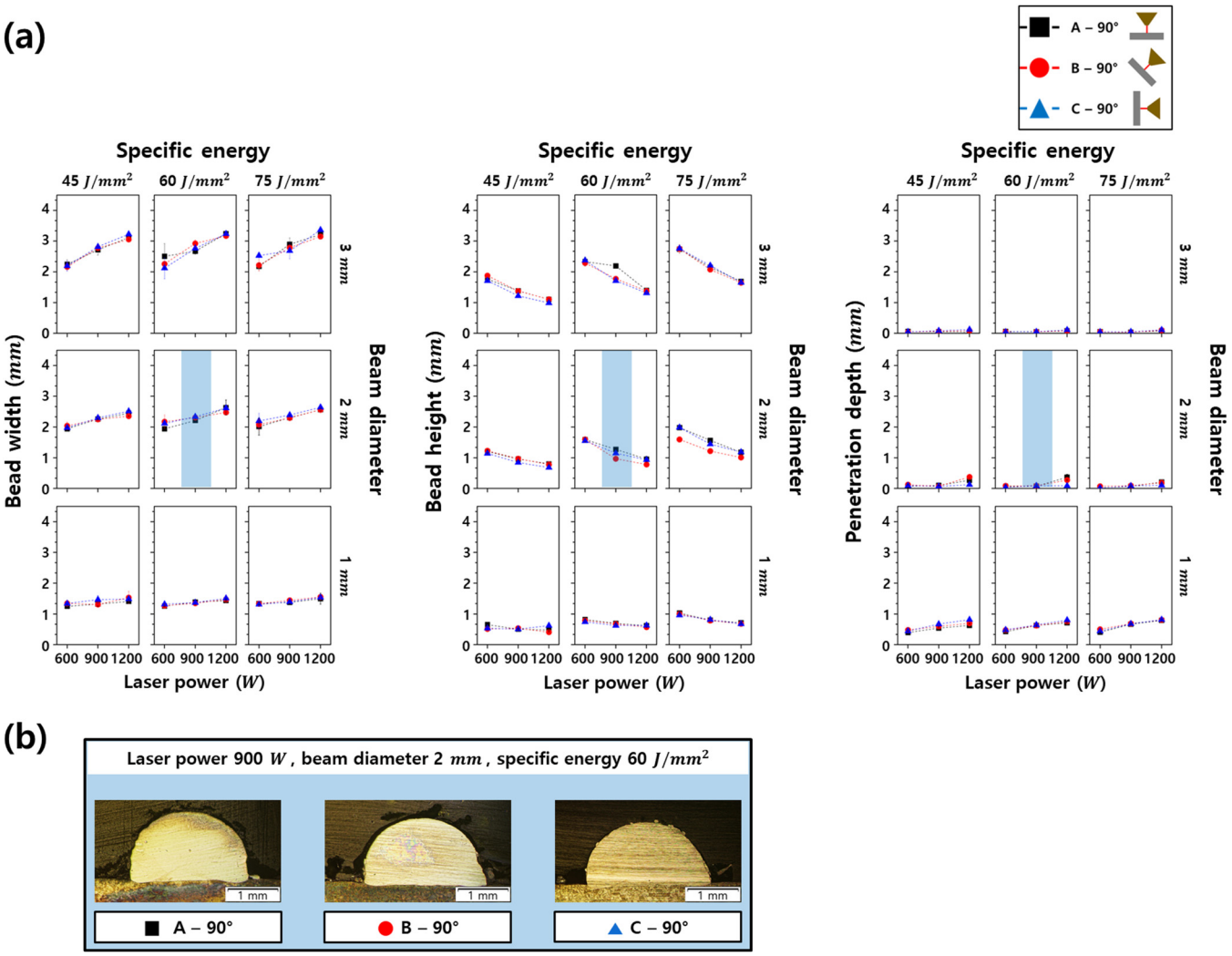

FIG. 6. Analysis and comparison of substrate tilting effect on bead cross-section geometry at A—90°, B—90°, and C—90°; (a) bead width, bead height, and penetration depth for A—90°, B—90°, and C—90°. (b) OM image of each spatial variable at laser power 900 W, beam diameter 2 mm, and specific energy of 60 J/mm^2.

from the OM image of a single-layer deposited under a processing variable set with each median value selected (laser power 900 W, beam diameter 2 mm, and specific energy of 60 J/mm^2). Therefore, based on this analysis, if θ was 90° during the multi-axis LMD process, the effect of gravitational force on the deposit's geometry was insignificant even when the substrate was tilted to a maximum of 90° from the ground, and various processing variables were used.

Deposition quality evaluation

In this study, the deposition quality of the single-layer, fabricated by using the multi-axis LMD process, was evaluated using the deposition quality evaluation indexes introduced in the previous section.

This study analyzed the effect of processing variables on the bead contact angle and dilution when the laser nozzle and substrate were not tilted (A—90°). In Figs. 7(a) and 7(b), the evaluation indexes were plotted under each processing variable set. As shown in Figs. 7(a) and 7(b), when the laser power increased, the left and right contact angles decreased while the dilution increased. This was because, as the laser power increased, bead width widened, and the area of the melted powder inside the substrate increased, which eventually led to a smaller contact angle and significant dilution. When the beam diameter was enlarged, dilution decreased because of the decrease in the amount of melted powder inside the substrate resulting from the lower heat energy distributed toward the substrate caused by the rise in the total amount of melted powder. Under fixed laser power and beam diameter conditions, as the

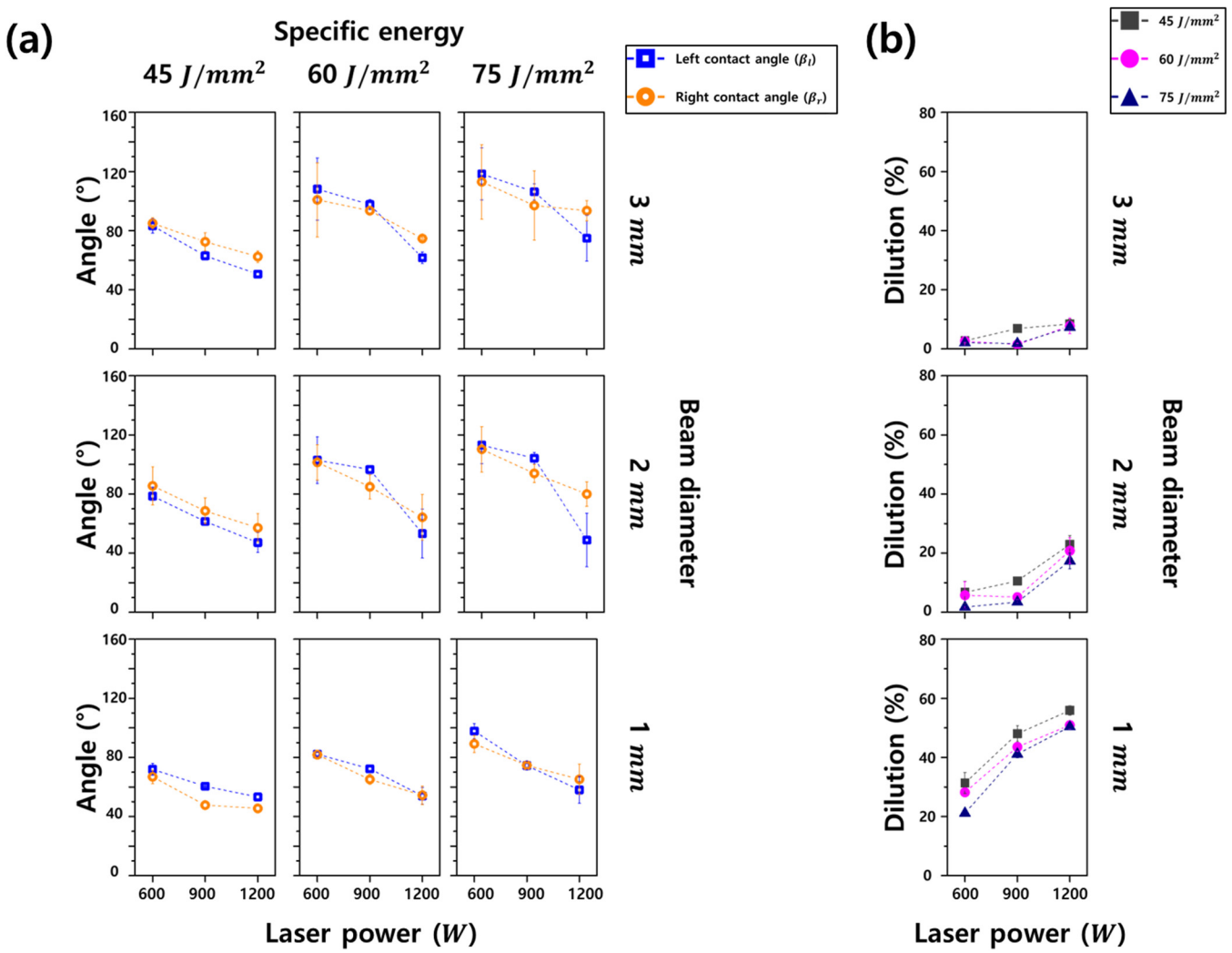

FIG. 7. Deposition quality evaluation indexes of the single-layer deposited at A—90°: (a) left and right contact angle and (b) dilution.

specific energy increased, the contact angle increased because of the decrease in the scanning speed, which led to a bead height increase.

Based on the correlation between the deposition quality evaluation indexes and the processing variables at A—90° as shown in Fig. 7, this study classified the bead cross-section geometry in six separate depending on how each geometry satisfied the ideal range of the contact angle and dilution. Each cross-section geometry was named ①–⑥.

1. Cross-section geometry ①, ②, ③ [Fig. 8(a)]: The contact angle was below 80°, which satisfied the ideal range, and in the order of ①, ②, and ③, the dilution was less than or equal to 10%, greater than 10% but less than 30% (ideal range), and greater than 30%.
2. Cross-section geometry ④, ⑤, ⑥ [Fig. 8(a)]: The contact angle was greater than 80°, and in the order of ④, ⑤, and ⑥, the dilution was less than or equal to 10%, greater than 10% but less than 30% (ideal range), and greater than 30%.

As shown in Fig. 8(a), ② satisfied every evaluation index's ideal range, therefore, ② had a geometry of superior deposition quality. However, during the multi-axis LMD process, when the laser nozzle and substrate are tilted using the same processing variable set, the deposit's cross-section geometry could be any one of ①, ③, ④, ⑤, and ⑥ instead of ②. Therefore, to investigate the effect of the laser nozzle and substrate tilting on the deposition quality, six cross-section geometries (①–⑥) were arranged in a table under every combination of the spatial and processing variables. Each cell was colored gray and sky-blue based on whether it

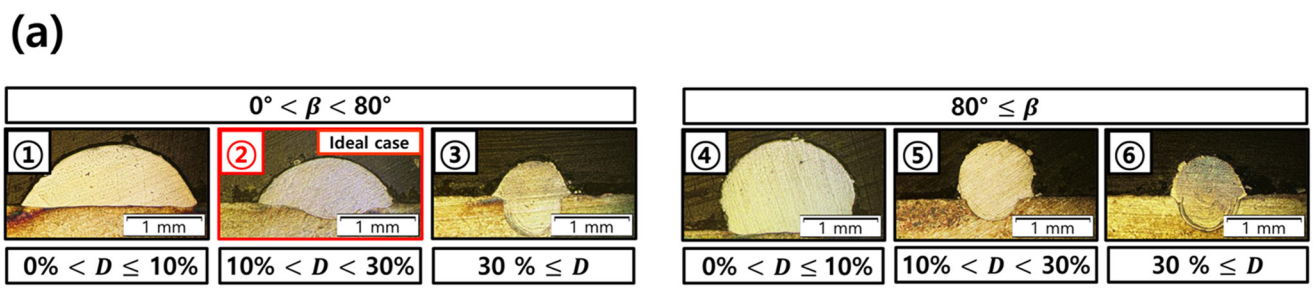

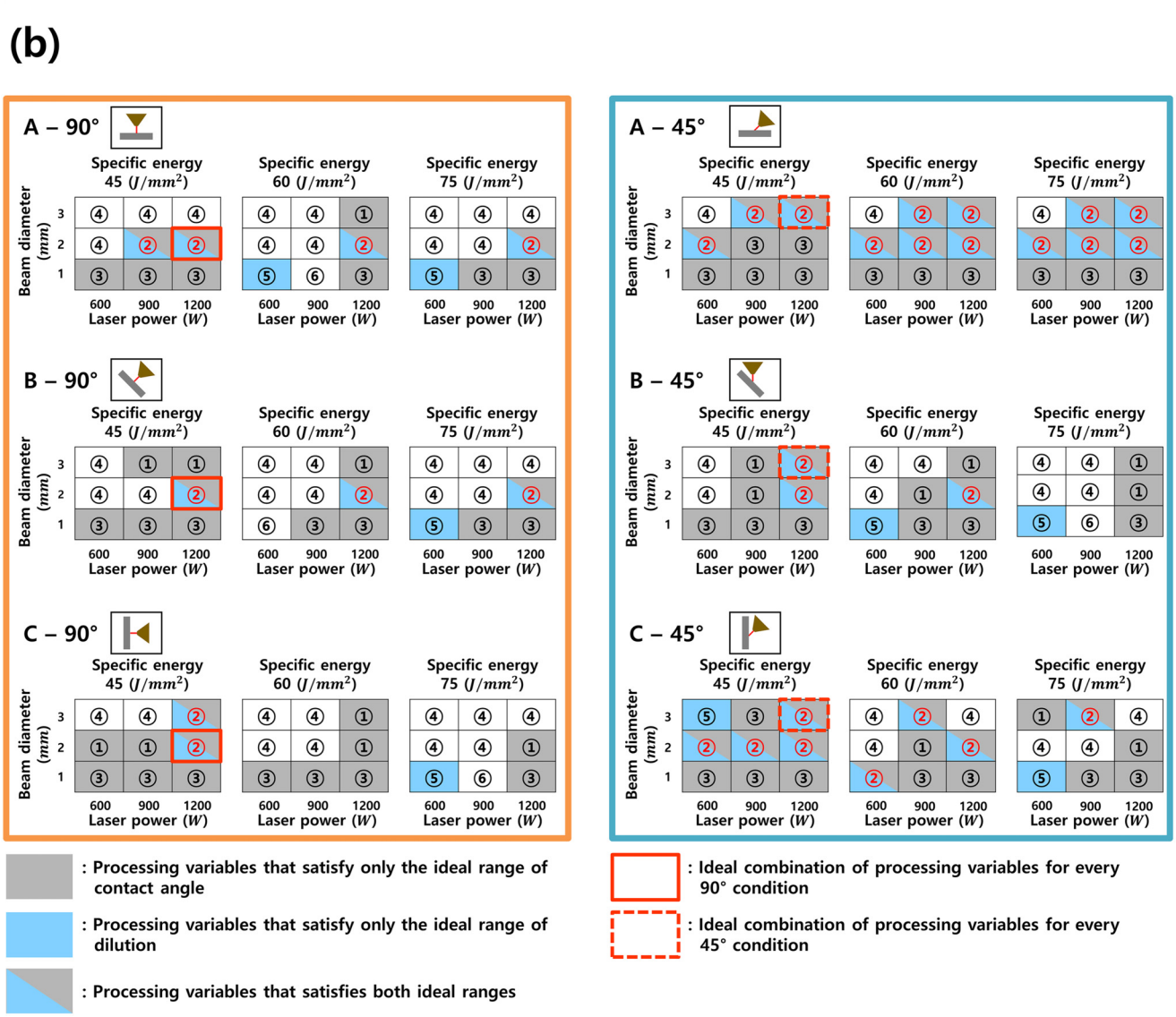

FIG. 8. Evaluation of the deposition quality under various spatial and processing variable sets. (a) Representative cross-section OM images of single-layer sorted under each evaluation indexes' ideal range (①: $0° < \beta < 80°$ and $0\% < D < 10\%$, ②: $0° < \beta < 80°$ and $10\% < D < 30\%$, ③: $0° < \beta < 80°$ and $30\% < D$, ④: $80° < \beta$ and $0\% < D < 10\%$, ⑤: $80° < \beta$ and $10\% < D < 30\%$, ⑥: $80° < \beta$ and $30\% < D$) (b) effect of spatial variable and processing variable on the evaluation indexes (For each processing variable set, the deposit's cross-section geometry is indicated and sets satisfying the contact angle and dilution's ideal range separately is colored grey and sky-blue, respectively. Both gray and sky-blue are colored for sets satisfying both the indexes' ideal ranges.).

satisfied each evaluation index's ideal range. The cell colored in gray and sky-blue represented ②, the ideal bead geometry.

When the substrate's posture was A, B, and C posture, at a beam diameter of 1 mm and specific energy of 45, 60, 75 J/mm^2, regardless of the laser nozzle tilting, when the laser power reached 1200 W, ③ appeared at every spatial variable, a geometry in which only the dilution exceeded the ideal range. At a beam diameter of 1 mm, ② only appeared at C—45° when the laser power was 600 W, and specific energy of 60 J/mm^2. The reason why ② appeared at only specific energy of 60 J/mm^2 was analyzed. At C—45°, when the laser power was 600 W, as the specific energy increased from 45 to 75 J/mm^2, the cross-section geometry changed in the order of ③, ②, and ⑤. Under the fixed laser power and beam diameter condition, the bead height increased proportionally with the specific energy because the scanning speed was decreased. Along with the bead height increase, the heat energy that was conducted toward the substrate decreased, which led to a lower dilution (③ dilution: 54%, ② dilution: 18%, ⑤ dilution: 14%) and a larger contact angle (③ contact angle: 36°, ② contact angle: 63°, ⑤ contact angle: 89°). Therefore, ② only appeared at specific energy of 60 J/mm^2 of laser power 600 W and beam diameter 1 mm. For other spatial variables except for C—45°, when laser power 600 W, beam diameter 1 mm, and specific energy of 60 J/mm^2 was used, A—90° and B—45° showed ⑤ in which only the contact angle exceeded 80°, and A—45°, B—90°, and C—90° showed ③ and ⑥ in which the dilution was greater than 30%. ② only appeared at C—45° in the following processing variable set because, as identified in Fig. 5(a), C—45° was the spatial variable in which the effect of laser nozzle tilting and the gravitational force on the bead geometry was most significant. Therefore, the powder melted widely in the direction of gravity, which was then solidified. This led to a smaller contact angle, and the low laser power (600 W) caused the amount of the powder melted on top of the substrate to be greater than the amount diluted inside the substrate, which referred to low dilution.

When a beam diameter of 2 mm and laser power of 1200 W was used, for θ at 90°, ① (dilution lower than 10%) and ② (ideal condition) appeared. For θ at 45° ③ (dilution greater than 30%) along with ① and ② occurred. For θ at 90°, ① only appeared at C—90° under specific energy of 60 and 75 J/mm^2. The reason for this was that at C—90°, unlike other spatial variables, the substrate was perpendicular to the ground at C—90° and the scanning speed was lower than the scanning speed at specific energy of 45 J/mm^2 with laser power 1200 W. When θ was 45°, ③ appeared at A posture under laser power 900 and 1200 W while the specific energy was 45 J/mm^2. In the other spatial variables of B—45° and C—45°, at laser power 900, 1200 W, and beam diameter 2 mm, ① and ②, conditions with dilution less than 30% appeared. This was because, unlike B—45° and C—45°, at A—45°, the substrate was not tilted from the ground, so the melted powder did not flow in the direction of the inclined substrate. Therefore, at A—45°, the powder's melted amount inside the substrate was greater than B—45° and C—45°, which led to a higher dilution.

For every spatial variable except for C—45°, when the beam diameter of 3 mm was used, as the laser power increased from 600 to 1200 W, dilution was almost held the same or increased. However, exceptionally at C—45° and a beam diameter of 3 mm, the dilution increased from 600 to 900 W and then decreased as the laser power was raised up to 1200 W. At that time, the change of cross-section geometry with respect to the laser power (in order of 600, 900, and 1200 W) for specific energy of 45 J/mm^2 was ⑤, ③, and ②, for specific energy 60 J/mm^2 was ④, ②, ④, and for specific energy of 75 J/mm^2 was ①, ②, and ④. The main reason for the difference in the cross-section geometry with accordance to the laser power for C—45° compared with every other spatial variable was related to the reason explained in Fig. 5 on why the bead height increased at 3 mm while the laser power increased from 900 W to 1200 W.

Based on all the information analyzed, the following conclusion could be derived in fabricating a component with excellent deposition quality when the laser nozzle and the substrate were tilted to build a component of complex geometry. For every substrate posture A, B, and C, when a beam diameter of 1 mm was used at a high laser power (1200 W), ③ in which only the dilution was greater than the ideal range was acquired. For a beam diameter of 2 mm and θ equaled to 90° at every substrate posture (A—90°, B—90°, and C—90°), the ideal cross-section geometry ② appeared commonly when laser power 1200 W and specific energy of 45 J/mm^2 [(Fig. 8(b) red line box] was used. When laser power 1200 W was used at high specific energy such as 60 and 75 J/mm^2, ② was shown at A—90° and B—90°. Using the identical laser power and specific energy levels, at C—90° in which the effect of gravity was high, ① with only the dilution smaller than 10% appeared. When a beam diameter of 3 mm was used, for θ equaled to 45° at every substrate posture (A—45°, B—45°, and C—45°), the ideal cross-section geometry ② appeared commonly when the laser power 1200 W and specific energy of 45 J/mm^2 were used [Fig. 8(b) red dotted line box]. Therefore, under fixed laser power and specific energy, if θ was 45°, components of excellent deposition quality could be made with a larger beam diameter than θ equaled to 90° at a high laser power and low specific energy.

CONCLUSION

This study analyzed the effects of the substrate's posture and laser nozzle tilting during the multi-axis LMD under various processing variables. Based on these results, the deposition guideline for fabricating a component with a superior deposition quality was established. Regardless of substrate and laser nozzle tilting, the amount of melted powder was low at a beam diameter of 1 mm. Thus, an excessive dilution occurred at a high laser power of 1200 W and at a beam diameter 1 mm condition. When a beam diameter of 2 mm was used for the condition in which the laser nozzle was perpendicular to the substrate of A, B, and C posture, at a high laser power of 1200 W and low specific energy of 45 J/mm^2, a single-layer structure of excellent deposition quality was fabricated. For a beam diameter of 3 mm condition, a component of high deposition quality during the condition in which the laser nozzle was tilted 45° from the substrate could be achieved at laser power 1200 W and specific energy of 45 J/mm^2 regardless of substrate posture. Therefore, a larger beam diameter can be more suitable for the laser nozzle tilted condition than not tilted condition in fabricating components of high deposition quality when high laser power and low specific energy are used. The above results can

help fabricate complex metal components with high precision and deposition qualities when using the multi-axis LMD process in various industrial fields, including the aerospace industry.

ACKNOWLEDGMENTS

The authors wish to acknowledge the tremendous and invaluable contributions that Jyoti Mazumder, who passed away on April 10, 2021, made to the field of laser materials processing. This work was mainly supported by the DN solutions Inc. of Korea, and the authors are grateful for the help. This work was also supported by the Technology Innovation Program (No. 20021982, Development of laser-based metal wire 3D printing technology to reduce thermal strain for high-speed/flexible production of aerospace and defense titanium parts) and the Korea Evaluation Institute of Industrial Technology (KEIT) (No. 20014796) grant funded by the Ministry of Trade, Industry & Energy (MOTIE, Korea).

AUTHOR DECLARATIONS

Conflict of Interest

The authors have no conflict to disclose.

Author Contributions

Dukyong Kim: Data curation (equal); Investigation (lead); Visualization (equal); Writing – original draft (lead). **Taehwan Ko:** Conceptualization (lead); Data curation (equal); Visualization (equal). **Seung Hwan Lee:** Funding acquisition (lead); Project administration (lead); Supervision (lead); Writing – review & editing (lead).

REFERENCES

[1]C. Selcuk, "Laser metal deposition for powder metallurgy parts," Powder Metall. **54**, 94–99 (2013).
[2]A. Vafadar, F. Guzzomi, A. Rassau, and K. Hayward, "Advances in metal additive manufacturing: A review of common processes, industrial applications, and current challenges," Appl. Sci. **11**, 1213 (2021).
[3]A. Pathania, S. Anand Kumar, B. K. Nagesha, S. Barad, and T. N. Suresh, "Reclamation of titanium alloy based aerospace parts using laser based metal deposition methodology," Mater. Today: Proc. **45**, 4886–4892 (2021).
[4]J. Jang, D. Van, and S. H. Lee, "Precipitation kinetics of secondary phases induced by heat accumulation in the deposit of Inconel 718," Additi. Manuf. **55**, 102831 (2022).
[5]J. Jiang, S. T. Newman, and R. Y. Zhong, "A review of multiple degrees of freedom for additive manufacturing machines," Int. J. Comput. Integr. Manuf. **34**, 195–211 (2021).
[6]J. Xu, X. Gu, D. Ding, Z. Pan, and K. Chen, "A review of slicing methods for directed energy deposition based additive manufacturing," Rapid Prototyp. J. **24**, 1012–1025 (2018).
[7]J. Hao, Q. Meng, C. Li, Z. Li, and D. Wu, "Effects of tilt angle between laser nozzle and substrate on bead morphology in multi-axis laser cladding," J. Manuf. Process. **43**, 311–322 (2019).
[8]G. Zhu, S. Shi, G. Fu, J. Shi, S. Yang, W. Meng, and F. Jiang, "The influence of the substrate-inclined angle on the section size of laser cladding layers based on robot with the inside-beam powder feeding," Int. J. Adv. Manuf. Technol. **88**, 2163–2168 (2017).
[9]P. Ramiro-Castro, M. Ortiz, A. Alberdi, and A. Lamikiz, "Effects of gravity and non-perpendicularity during powder-fed directed energy deposition of Ni-based alloy 718 through two types of coaxial nozzle," Metals **10**, 560 (2020).
[10]J. Park, J.-Y. Kim, I. Ji, and S. H. Lee, "Numerical and experimental investigations of laser metal deposition (LMD) using STS 316L," Appl. Sci. **10**, 4874 (2020).
[11]J. Park and S. H. Lee, "CMT-based wire arc additive manufacturing using 316L stainless steel (2): Solidification map of the multilayer deposit," Metals **11**, 1725 (2021).
[12]B. Chen, Y. Su, Z. Xie, C. Tan, and J. Feng, "Development and characterization of 316L/Inconel625 functionally graded material fabricated by laser direct metal deposition," Opt. Laser Technol. **123**, 105916 (2020).
[13]S. Pratheesh Kumar, S. Elangovan, R. Mohanraj, and J. R. Ramakrishna, "A review on properties of Inconel 625 and Inconel 718 fabricated using direct energy deposition," Mater. Today: Proc. **46**, 7892–7906 (2021).
[14]S. W. Yang, J. Yoon, H. Lee, and D. S. Shim, "Defect of functionally graded material of Inconel 718 and STS 316L fabricated by directed energy deposition and its effect on mechanical properties," J. Mater. Res. Technol. **17**, 478–497 (2022).
[15]Y. Kim, H. Nam, J. Lee, C. Park, B. Moon, D.-G. Nam, S. H. Lee, and N. Kang, "Hot-cracking resistivity of dissimilar clads using Inconel 52 and 308L stainless steel on carbon steel," J. Nucl. Mater. **533**, 152103 (2020).
[16]B. Z. Xinwei Wu, Xiaoyan Zeng, Xiang Hu, and Kun Cui, "Critical state of laser cladding with powder auto-feeding," Surf. Coat. Technol. **79**, 200–204 (1996).
[17]T. E. Abioye, J. Folkes, and A. T. Clare, "A parametric study of Inconel 625 wire laser deposition," J. Mater. Process. Technol. **213**, 2145–2151 (2013).
[18]Y. Huang, M. B. Khamesee, and E. Toyserkani, "A new physics-based model for laser directed energy deposition (powder-fed additive manufacturing): from single-track to multi-track and multi-layer," Opt. Laser Technol. **109**, 584–599 (2019).
[19]R. M. Mahamood, "Effect of laser power and powder flow rate on dilution rate and surface finish produced during laser metal deposition of titanium alloy," in *8th International Conference on Mechanical and Intelligent Manufacturing Technologies, Cape Town, South Africa, 3–6 February 2017* (IEEE Explore, 2017).